npj | Quantum Materials

www.nature.com/npjquantmats

ARTICLE OPEN

f-electron hybridised Fermi surface in magnetic field-induced metallic YbB_{12}

H. Liu[1,8], A. J. Hickey[1,8], M. Hartstein[1], A. J. Davies[1], A. G. Eaton[1], T. Elvin[1], E. Polyakov[1], T. H. Vu[1], V. Wichitwechkarn[1], T. Förster[2], J. Wosnitza[2,3], T. P. Murphy[4], N. Shitsevalova[5], M. D. Johannes[6], M. Ciomaga Hatnean[7], G. Balakrishnan[7], G. G. Lonzarich[1] and Suchitra E. Sebastian[1]✉

The nature of the Fermi surface observed in the recently discovered family of unconventional insulators starting with SmB_6 is a subject of intense inquiry. Here we shed light on this question by accessing quantum oscillations in the high magnetic field-induced metallic regime above ≈47 T in YbB_{12}, which we compare with the unconventional insulating regime. In the field-induced metallic regime, we find prominent quantum oscillations in the electrical resistivity characterised by multiple frequencies and heavy effective masses. The close similarity in Lifshitz-Kosevich low-temperature growth of quantum oscillation amplitude in insulating YbB_{12} to field-induced metallic YbB_{12}, points to an origin of quantum oscillations in insulating YbB_{12} from in-gap neutral low energy excitations. Higher frequency Fermi surface sheets of heavy quasiparticle effective mass emerge in the field-induced metallic regime of YbB_{12} in addition to multiple heavy Fermi surface sheets observed in both insulating and metallic regimes. *f*-electron hybridisation is thus observed to persist from the unconventional insulating to the field-induced metallic regime of YbB_{12}, in contrast to the unhybridised conduction electron Fermi surface observed in unconventional insulating SmB_6. Our findings thus require an alternative model for YbB_{12}, of neutral in-gap low energy excitations, wherein the *f*-electron hybridisation is retained.

npj Quantum Materials (2022)7:12 ; https://doi.org/10.1038/s41535-021-00413-7

INTRODUCTION

The origin of bulk quantum oscillations in bulk insulating unconventional insulators, first discovered in SmB_6[1], has been the subject of much debate[1–7]. Another recently discovered unconventional insulator is the Kondo insulator YbB_{12}[4,5], in which high magnetic fields dramatically reduce the electrical resistivity, causing the metallic ground state to be realised beyond $\mu_0 H \approx 47$ T[8,9]. Quantum oscillation measurements in metallic YbB_{12} accessed in high magnetic fields thus uniquely enable us to make a comparison between quantum oscillations in the unconventional insulating state and the field-induced metallic state.

In this paper, we experimentally compare quantum oscillations in the unconventional insulating regime and the field-induced metallic regime of YbB_{12} accessed through high applied magnetic fields up to 68 T. In the field-induced metallic phase of YbB_{12}, we observe prominent quantum oscillations with a multiplicity of frequencies characterised by moderately heavy quasiparticle effective masses, which reflect an *f*-electron hybridised metallic Fermi surface. In order to reliably extract information from the complex quantum oscillation spectrum comprising multiple frequencies, we focus on (i) a comparison of the multiple quantum oscillation frequencies observed in both magnetic torque and electrical resistivity of the unconventional insulating regime[4] and contactless resistivity of the field-induced metallic regime, (ii) the temperature dependent quantum oscillation amplitude that can be used to distinguish between gapped and gapless Fermi surface models in the unconventional insulating regime, and (iii) consequently shed light on the nature of hybridisation in the unconventional insulating and field-induced metallic regimes.

RESULTS

Quantum oscillations in field-induced metallic YbB_{12}

Figure 1 a shows quantum oscillations in the contactless electrical resistivity of a single crystal of YbB_{12} measured using the proximity detector oscillator (PDO) technique, at high magnetic fields above the insulator-metal transition at $\mu_0 H \approx$ 47 T[9]. Prominent quantum oscillations are visible in the measured contactless electrical resistivity before background subtraction. Figure 1b shows quantum oscillations after smooth, monotonic backgrounds have been subtracted from the contactless electrical resistivity (measured by the resonant frequency) above 50 T at various temperatures, where the quantum oscillation periodicity in inverse magnetic field can be seen. Multiple frequency peaks between 500(200) and 3000(200) T are revealed by Fast Fourier Transforms (FFT) of the background-subtracted quantum oscillations, as shown in Fig. 2a. Plotting the quantum oscillation amplitude as a function of temperature down to 0.6 K yields a Lifshitz-Kosevich (LK) temperature dependence with cyclotron effective masses m^*/m_e between 8.5(1) znd 17(3), as shown in Fig. 2b.

DISCUSSION

Figure 3 shows multiple quantum oscillation frequencies in the insulating phase of YbB_{12} measured through capacitive magnetic

[1]Cavendish Laboratory, University of Cambridge, JJ Thomson Avenue, Cambridge CB3 0HE, UK. [2]Dresden High Magnetic Field Laboratory (HLD-EMFL) and Würzburg-Dresden Cluster of Excellence ct.qmat, Helmholtz Zentrum Dresden Rossendorf, Bautzner Landstrasse 400, Dresden 01328, Germany. [3]Institut für Festkörper- und Materialphysik, Technische Universität Dresden, Dresden 01062, Germany. [4]National High Magnetic Field Laboratory, Tallahassee, FL 32310, USA. [5]The National Academy of Sciences of Ukraine, Kiev 03680, Ukraine. [6]Center for Computational Materials Science, Naval Research Laboratory, Washington, DC 20375, USA. [7]Department of Physics, University of Warwick, Coventry CV4 7AL, UK. [8]These authors contributed equally: H. Liu, A. J. Hickey. ✉email: suchitra@phy.cam.ac.uk

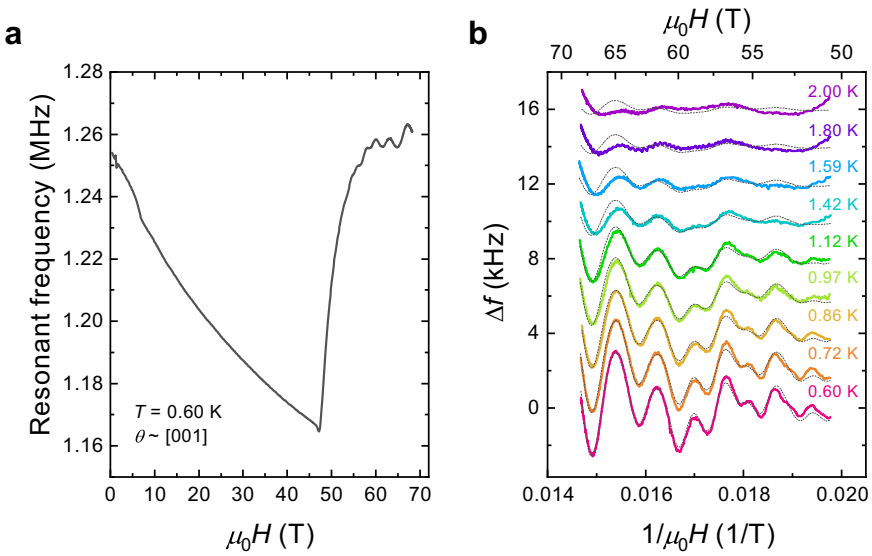

Fig. 1 Quantum oscillations in the field-induced metallic phase of YbB_{12}. Electrical resistivity of a single crystal of YbB_{12} measured with the contactless proximity detector oscillator (PDO) technique. **a** PDO resonant frequency as a function of applied magnetic field up to 68 T at a temperature of 0.60 K with the field aligned close to the [001] crystallographic direction. The sharp change in resonant frequency at $\mu_0 H \approx 47$ T indicates the onset of the insulator-metal transition[8,9]. Prominent oscillations can be seen against the unsubtracted background above $\mu_0 H \approx 50$ T. **b** Solid lines show quantum oscillations measured with PDO up to 68 T with a smooth monotonic background subtracted at different temperatures, where Δf is the change in resonant frequency after background subtraction. Dashed lines show Lifshitz-Kosevich simulations of quantum oscillations using multiple frequency components as listed in Table 1.

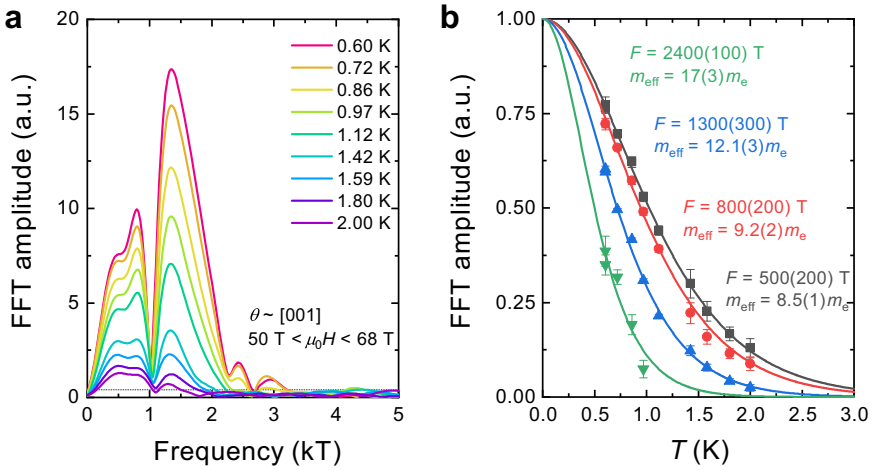

Fig. 2 Rich spectrum of multiple quantum oscillation frequencies in the field-induced metallic phase of YbB_{12}. a Fourier transforms of the subtracted quantum oscillations shown in Fig. 1b, for a field window of 50T < $\mu_0 H$ < 68T at temperatures between 0.6 and 2.0 K, where the applied field was aligned close to the [001] crystallographic direction. The horizontal dashed line indicates the FFT noise floor. Multiple distinct quantum oscillation frequency peaks between 500(200) and at least 3000(200) T are visible. **b** Quantum oscillation amplitude obtained from the Fourier transform peak height shown in (**a**) as a function of temperature for multiple representative frequencies. Lifshitz–Kosevich temperature dependence fits, as shown by the solid lines, yield quasiparticle effective masses m^*/m_e between 8.5(1) and 17(3) for the various frequencies. A summary of the multiple observed frequencies and their corresponding effective masses is shown in Table 1.

torque and contacted electrical transport[4]. Figure 2a shows the quantum oscillation frequency spectrum in the field-induced metallic phase, comprising multiple frequencies extending up to at least 3000(200) T. We note that even higher frequencies may exist, especially in view of the high value of linear specific heat $\gamma \approx 67$ mJ mol^{-1} K^{-2} measured in the field-induced metallic regime of YbB_{12}[10]. Multiple comparable quantum oscillation frequencies between ~300 and 800 T are measured in both the metallic and insulating phases (Table 1); the multiple frequencies measured by magnetic torque in the insulating phase of YbB_{12} had previously been reported, which, through a comparison of the absolute amplitude of quantum oscillations with the expectation from the bulk volume in the infinite field limit, and the observation that more insulating samples exhibit larger amplitude quantum oscillations, have been shown to be intrinsic to the insulating bulk of YbB_{12}[4]. Curiously, these multiple frequencies were missed in other reports of a single quantum oscillation frequency in the insulating phase of YbB_{12}[5]. Such a quantum oscillation spectrum comprising multiple frequencies is expected from numerical Fermi surface simulations of metallic YbB_{12} involving hybridised *f*-electrons[4]. In these theoretical simulations of the Fermi surface, multiple Fermi surface pockets located away from the centre of the Brillouin zone would be expected to yield a series of frequency branches; multiple frequencies would further be expected from a multiplicity of

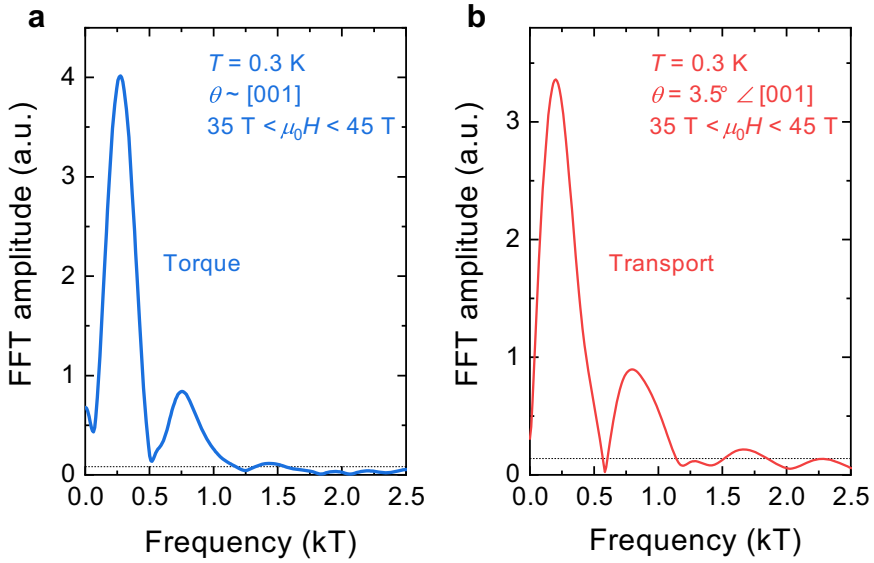

Fig. 3 FFT of quantum oscillations in insulating YbB_{12}. FFT of quantum oscillations measured on insulating YbB_{12} at a temperature of 0.3 K and field range of 35 T < $\mu_0 H$ < 45 T in (**a**) magnetic torque, with the applied field aligned close to the [001] crystallographic direction, and (**b**) electrical resistivity, with the applied field aligned 3.5° away from the [001] crystallographic direction in the [001]-[111]-[110] rotation plane. The horizontal dashed lines indicate the FFT noise floors. Similar frequencies can be discerned in the two measured physical quantities. A summary of the multiple observed frequencies and their respective quasiparticle effective masses is shown in Table 1. An FFT decomposition involving LK simulations identifies a frequency ≈ 450 T in electrical resistivity that is visible as a shoulder of the main peak.

Table 1. Observed multiple quantum oscillation frequencies and effective masses in the insulating and metallic phases of YbB_{12}.

Insulating phase				Metallic phase	
Frequency (T)	Mass (m_e)	Frequency (T)	Mass (m_e)	Frequency (T)	Mass (m_e)
dHvA ($\theta \sim$ [001])		SdH ($\theta = 3.5° \angle$ [001])		PDO ($\theta \sim$ [001])	
		150 (90)	3.2 (2)		
300 (70)	4.5 (5)	450 (80)	6.1 (6)	500 (200)	8.5 (1)
700 (90)	7 (2)	800 (90)	7.9 (8)	800 (200)	9.2 (2)
				1300 (200)	12.1 (3)
				1700 (200)	16 (5)
				2300 (200)	17 (3)
				3000 (200)	14 (3)

Multiple quantum oscillation frequencies and cyclotron effective masses measured with capacitive torque magnetisation (de Haas-van Alphen (dHvA) oscillations) and four-point contacted resistivity (Shubnikov-de Haas (SdH) oscillations) in the insulating phase of YbB_{12}, and with proximity detector oscillator (PDO) contactless electrical transport in the magnetic field-induced metallic phase of YbB_{12}. The applied magnetic field was aligned close to the [001] crystallographic direction for dHvA and PDO measurements, and was aligned 3.5° from the [001] crystallographic direction in the [001]-[111]-[110] rotational plane for the SdH measurements. The FFT field range was 50 T < $\mu_0 H$ < 68 T for PDO, 25 T < $\mu_0 H$ < 45T for the 700 T frequency in dHvA, 35 T < $\mu_0 H$ < 45 T for the 800 T frequency in SdH, and 28 T < $\mu_0 H$ < 45 T for other frequencies in dHvA and SdH. For contacted resistivity in the insulating phase, we subtract away a smooth monotonic polynomial resistivity background at each temperature and use the relative change in resistivity to determine the quantum oscillation amplitude as a function of temperature. The effective mass obtained from contacted resistivity and magnetic torque quantum oscillations for similar frequencies are in good agreement.

electron and hole pockets. Fourier analysis in the high magnetic field range over which we measure quantum oscillations in this work reveals a complex spectrum in the metallic phase comprising a large number of constituent frequencies with similar amplitudes (shown in Fig. 2), rendering inappropriate analysis methods such as Landau level indexing assuming a single dominant frequency. In this work, therefore, we focus instead on a robust treatment involving comparison between the multiple quantum oscillation frequencies identified by Fourier transforms, and the temperature-dependence of the quantum oscillation amplitudes corresponding to these multiple frequencies observed in both the unconventional insulating[4] and field-induced metallic regimes.

Broad classes of models that have been proposed to explain bulk quantum oscillations in unconventional insulators include categories of gapped models, and models characterised by in-gap low energy excitations[11–23]. An analysis of the temperature-dependence of the quantum oscillation amplitude provides us with vital information to distinguish between classes of gapped and gapless models to describe quantum oscillations in the unconventional insulating phase.

At the simplest level of weakly interacting gapped systems, these systems are characterised by a single particle gap. Models in this category have for example been proposed for BCS superconductors[11] and for weakly interacting insulators[12,13]. For this category of gapped models of quantum oscillations in weakly interacting insulators, the quantum oscillation amplitude exhibits a non-LK flattening or decrease at low temperatures[11,12] (Supplementary Information, Fig. 4a lower inset). Other models of weakly interacting gapped systems invoke quantum oscillations arising from modulation of the gap resulting from an inverted band structure[14–16].

This picture is modified in the case of strongly correlated insulators. The emergence of an in-gap density of states has been modelled by various theories applicable to these insulators that are driven by strong interactions. For instance, models of single-band Mott insulators[18,19] involve low energy excitations of chiefly spin character. Models of Majorana fermions proposed for Kondo insulators include those in refs. [20–22]. In these models, low energy excitations involve Majorana fermion bands, that can be a linear equal combination of a canonical particle and anti-particle operators, crossing the chemical potential. Another model has been proposed for quantum oscillations from composite fermionic excitons in Kondo insulators[23]. In this case, mixed-valence insulators are proposed to host a fractionalised neutral Fermi

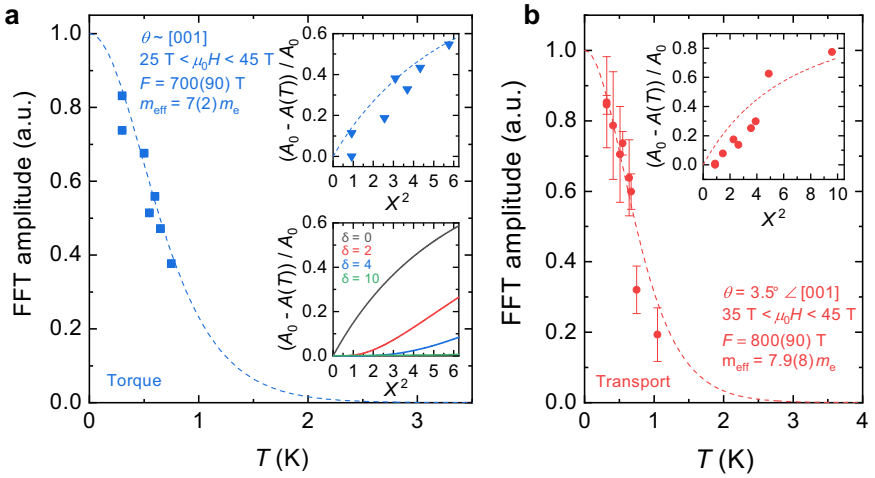

Fig. 4 Gapless low energy excitations yield low temperature Lifshitz-Kosevich growth of quantum oscillation amplitude in the insulating phase of YbB_{12}. **a** Amplitude of the 700 T frequency quantum oscillations measured using cantilever torque magnetometry as a function of temperature, with the applied field aligned close to the [001] crystallographic direction. Measured quantum oscillation amplitude follows the Lifshitz-Kosevich (LK) form (dashed line) down to lowest measured temperatures. (Lower inset) Low temperature model expansion of quantum oscillation amplitude from refs. [11,12] shows non-LK activated behaviour for various finite gap sizes ($\delta \approx 12$ for YbB_{12} at 40 T[8]), in contrast to LK exponential growth expected for gapless low energy excitations ($\delta = 0$). Model calculations are shown in Supplementary Information. $A(T)$ is the quantum oscillation amplitude at temperature T, A_0 is the amplitude at the lowest measured temperature, $X = 2\pi^2 k_B T/\hbar\omega_c$ is the temperature damping coefficient in the LK formula[35], $\delta = 2\pi\Delta/\hbar\omega_c$ where Δ is the isotropic gap size and ω_c is the cyclotron frequency. (Upper inset) Growth of magnetic torque quantum oscillation amplitude at the lowest measured temperatures; experimental data (solid triangles) exhibits good agreement with gapless model simulation (dashed lines). **b** Amplitude of the 800 T frequency quantum oscillations measured using four-point contacted electrical transport as a function of temperature, with the applied field aligned 3.5° away from the [001] crystallographic direction in the [001]-[111]-[110] rotation plane. Measured quantum oscillation amplitude follows LK form (dashed line) down to lowest measured temperatures. (Inset) Growth of electrical transport quantum oscillation amplitude at lowest temperatures; experimental data (solid circles) exhibits good agreement with gapless model simulation (dashed line).

sea, which develops an emergent magnetic field in the presence of a physical magnetic field. The quantum oscillation amplitude in these gapless models is expected to increase at low temperatures, for instance obeying an LK form in the case of low energy excitations characterised by Fermi-Dirac statistics (Supplementary Information, Fig. 4a lower inset). It is also of interest to consider the case of unconventional superconductors, in which quantum oscillations are experimentally observed in the vortex regime[24–28]; quantum oscillations in a Kondo insulator may arise in a regime potentially analogous to such a vortex state, but one in which the two-component collective hybridisation order parameter of the Kondo lattice could play a role similar to the two-component superconducting order parameter.

Figure 2 shows the quantum oscillation amplitude as a function of temperature in field-induced metallic YbB_{12}, growing in accordance to the LK form down to the lowest measured temperatures, as expected for a metal characterised by Fermi-Dirac statistics. We obtain the cyclotron effective mass for multiple quantum oscillation frequencies in the field-induced metallic phase of YbB_{12} from an LK fit to the quantum oscillation amplitude as a function of temperature (Fig. 2b). Table 1 shows a range of moderately high effective masses m^*/m_e up to at least 17(3) observed for multiple quantum oscillation frequencies up to at least 3000(200) T. The heavy effective masses observed in the field-induced metallic phase indicate its correspondence to an *f*-electron hybridised metallic Fermi surface[10].

The presence of low-energy excitations in the gap that do not participate in longitudinal charge transport would be expected to yield an increase in quantum oscillation amplitude at low temperatures in strongly correlated models, which distinguishes them from gapped models of quantum oscillations in weakly interacting insulators in which the quantum oscillation amplitude is expected to exhibit non-LK flattening or decrease at low temperatures[11,12] (Supplementary Information, Fig. 4a lower inset). Figure 4 shows the temperature dependence of quantum oscillation amplitude for multiple representative frequencies in magnetic torque and electrical transport measured in the insulating phase of YbB_{12}[4]. Similar to our observation in the metallic phase, the quantum oscillation amplitude of both magnetic torque and electrical resistivity in the insulating phase grows in accordance with the LK form down to the lowest measured temperatures, below the gap temperature beneath which gapped models of quantum oscillations predict a non-LK flattening or decrease in amplitude[11,12]. LK fits to the quantum oscillation amplitude as a function of temperature of quantum oscillation frequencies between 300 and 800 T observed in the insulating phase yield moderately heavy effective masses m^*/m_e between ~4.5 and 9, which are similar to the effective masses observed in the field-induced metallic phase for a similar range of quantum oscillation frequencies (Table 1). The growth in quantum oscillation amplitude down to the lowest measured temperatures is clearly evidenced in the two upper insets in Fig. 4, which highlight low temperature growth of the torque and transport quantum oscillation amplitude measured in the insulating phase. This striking observation of a steep increase in quantum oscillation amplitude down to the lowest temperature is in clear contrast to the non-LK flattening or decrease expected for gapped Fermi surface models, a simulation of which is shown in the lower inset of Fig. 4 for various gap values, exhibiting non-LK finite activation behaviour for a finite gap. We are thus able to identify quantum oscillation signatures in the unconventional insulator YbB_{12} that reveal an origin from low-energy excitations in the gap that do not participate in longitudinal charge transport, as yielded by correlated insulator models.

Our comparison of measured quantum oscillations between the unconventional bulk insulating regime[4] and field-induced metallic regime of YbB_{12} shows that an application of magnetic fields yields a spectrum of multiple quantum oscillation frequencies that appear prominently in magnetic field-induced metallic YbB_{12}, encompassing similar frequencies below 1000 T observed in

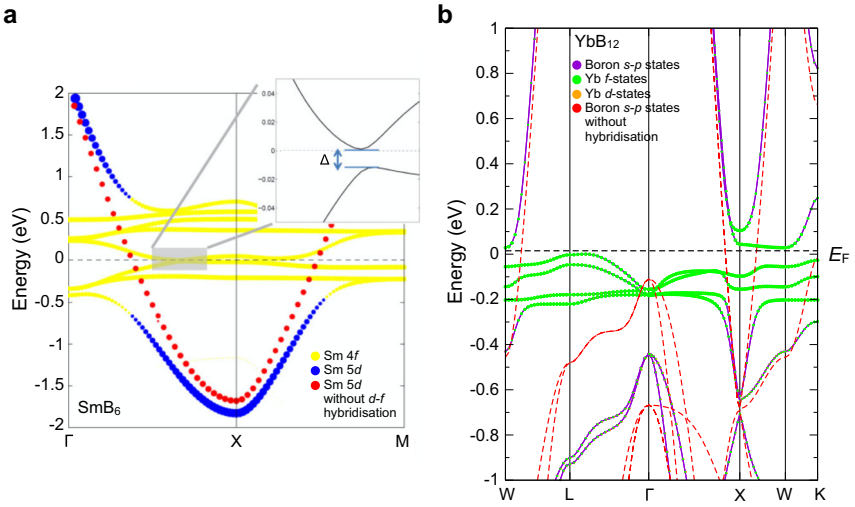

Fig. 5 Contrasting band structure of SmB_6 and YbB_{12}. **a** Band structure of SmB_6 from GGA calculations in ref. [36], zoomed in view near the Fermi energy E_F (full energy range shown in ref. [36]). Sizes of yellow and blue dots denote weights of Sm-4*f* and Sm-5*d* in various bands. Red dots denote metallic Sm-5*d* orbitals without hybridisation with Sm-4*f* orbitals. **b** Calculated band structure of YbB_{12} shown with an expanded view around the Fermi energy E_F (full energy range shown in ref. [4]). Size of the circles are proportional to the weight at each *k*-point, green circles are Yb *f*-states, orange circles are Yb *d*-states, and violet circles are boron *s-p*-states. Red dots denote two partially filled unhybridised boron *s-p* conduction electron orbitals without hybridisation with Yb-*f* orbitals. In both cases, the Fermi surface yielded by the unhybridised band is not simply connected, leading to a large number of expected frequencies[1,4].

insulating YbB_{12}, but extending to higher frequencies up to at least 3000(200) T (Table 1). The comparable quantum oscillation frequency range observed in both metallic and insulating regimes is characterised by similar moderately heavy effective masses in both regimes, while higher frequencies in the field-induced metallic phase are characterised by heavy effective masses m^*/m_e up to at least 17(3). This appearance of multiple additional heavy Fermi surface sheets in the magnetic field-induced metallic regime of YbB_{12} would explain the steep increase in the linear specific heat at the field-induced insulator metal transition reported in ref. [10].

Our observation of a heavy Fermi surface with multiple quantum oscillation frequencies in the unconventional insulating and high field-induced metallic regimes of YbB_{12} points to a multi-component Fermi surface characterised by *f*-electron hybridisation that persists from the unconventional insulating regime to the high field metallic regime. We note a crucial distinction between the band structure of unconventional insulators SmB_6[1] and YbB_{12}[4]. While in the case of SmB_6, a single half-filled unhybridised conduction *d*-electron band crosses the Fermi energy and hybridises with the *f*-electron band to yield the Kondo gap (Fig. 5a), the situation is different in YbB_{12}. In the case of YbB_{12}, two partially filled unhybridised *s-p* conduction electron bands that are cumulatively half-filled cross the Fermi energy with electron-like character, and are gapped by hybridisation with the *f*-electron band (Fig. 5b). We find this difference leads to a distinct contrast between the case of the unconventional insulator YbB_{12}, where heavy Fermi surface sheets are characterised by *f*-electron hybridisation, and the case of SmB_6, in which the observed light Fermi surface sheets correspond to an unhybridised conduction electron band[1]. Our findings in YbB_{12} are a challenge to correlated models of in-gap states that are expected to yield a Fermi surface corresponding to an unhybridised conduction electron band. An alternative possibility is suggested by the close proximity of the underlying bandstructure to a semimetallic bandstructure comprising heavy *f*-electron hybridised electron and hole pockets (Fig. 5). For weak correlations between electrons and holes, metallic electrical conduction would be expected. In contrast, for strong correlations, the electrons and holes may be expected to combine, such that they cannot be readily decoupled, thus impeding longitudinal electrical conduction. Despite the electrically insulating behaviour in such a strongly correlated case where electrons and holes are coupled, the Lorentz force could potentially still drive orbital currents, which would yield quantum oscillations corresponding to a heavy *f*-electron hybridised semimetallic Fermi surface of the kind observed.

METHODS

Sample preparation

Source polycrystalline YbB_{12} powder was synthesised using borothermal reduction of 99.998% mass purity Yb_2O_3 powder and 99.9% mass purity amorphous B at 1700 °C under vacuum[29]. The synthesised powder was isostatically pressed into a cylindrical rod and sintered at 1600 °C in Ar gas flow for several hours. Single crystals of YbB_{12} were grown by the travelling solvent floating zone technique under conditions similar to those in ref. [30] using a four-mirror Xe arc lamp (3 kW) optical image furnace from Crystal Systems Incorporated, Japan. The growths were performed in a reducing atmosphere of Ar with 3% H_2 at a rate of 18 mm hr^{-1} with the feed and seed rods counter-rotating at 20–30 rpm. Samples for all measurement techniques were cut to size using a wire saw and electropolished to remove heat damage and surface strain.

Proximity detector oscillator

Contactless electrical transport measurements using the proximity detector oscillator (PDO) technique[31] were performed using a long-pulse magnet capable of generating up to 68 T at the Hochfeld Magnetlabor Dresden (HLD) in Dresden, Germany. The capacitor bank-driven magnet has a pulse duration of 150 ms, and is fitted with a custom made ^{3}He system with a base temperature of ≈600 mK. The PDO circuit was made in accordance to ref. [31], using a hand-wound sensing coil with 10 turns. The raw frequency output from the PDO circuit was ~20 MHz, which was passed through a processing circuit before being recorded at ~1 MHz using a National Instruments PXI system recording at 15 MHz.

Capacitive torque magnetometry

Torque magnetometry measurements were performed in DC magnetic fields at the National High Magnetic Field Laboratory in Tallahassee,

Florida, USA. The 45 T hybrid magnet was operated with a ^{3}He system capable of reaching temperatures as low as 300 mK.

Cantilevers were cut from 20 μm or 50 μm thick pieces of BeCu into flexible T-shaped pieces. Samples of dimensions approximately $1 \times 1 \times 0.5$ mm^3 were secured on the wide end of the cantilever using epoxy, which was thermally matched to the sample to minimise strain. The narrow end of the cantilever was secured down such that the wide end of the cantilever hovers above a Cu baseplate, forming the two plates of a capacitor. The change in capacitance between the two plates was measured using a General Radio analogue capacitance bridge with a lock-in amplifier.

Density functional theory calculations

Density functional theory bandstructures were calculated with the Wien2k augmented plane wave plus local orbital (APW+lo) code[32]. The modified Becke-Johnson (mBJ) potential was used, which is a semi-local approximation to the exact exchange plus a screening term[33] and which improves the band gap in many semiconductor materials. Application of mBJ resulted in a non-magnetic ground state with an indirect band gap of 21 meV and a direct gap of 80 meV, whereas the standard Perdew Burke Ernzerhof (PBE) potential produced a semimetal with overlapping valence and conduction bands. Spin-orbit coupling was included via the second variational method and resulted in a strong reordering of the bands. Self-consistent calculations were converged using a k-mesh of $15 \times 15 \times 15$ followed by a non-self-consistent calculation with a $30 \times 30 \times 30$ mesh for calculation of Fermi surfaces. The bandstructure for boron *s-p* states without hybridisation was calculated by shifting the *f*-bands out of the energy range of hybridisation using DFT + U[34].

DATA AVAILABILITY

All data are included in the manuscript. Supporting data are available from the corresponding author upon reasonable request.

Received: 2 March 2021; Accepted: 10 December 2021;
Published online: 21 January 2022

REFERENCES

1. Tan, B. S. et al. Unconventional Fermi surface in an insulating state. *Science.* **349**, 287–290 (2015).
2. Hartstein, M. et al. Fermi surface in the absence of a Fermi liquid in the Kondo insulator SmB_6. *Nat. Phys.* **14**, 166–172 (2018).
3. Li, G. et al. Two-dimensional Fermi surfaces in Kondo insulator SmB_6. *Science.* **346**, 1208–1212 (2014).
4. Liu, H. et al. Fermi surfaces in Kondo insulators. *J. Phys. Condens. Matter* **30**, 16LT01 (2018).
5. Xiang, Z. et al. Quantum oscillations of electrical resistivity in an insulator. *Science* **362**, 65–69 (2018).
6. Wang, P. et al. Landau quantization and highly mobile fermions in an insulator. *Nature* **589**, 225–229 (2021).
7. Hartstein, M. et al. Intrinsic bulk quantum oscillations in a bulk unconventional insulator SmB_6. *iScience* **23**, 101632 (2020).
8. Sugiyama, K., Iga, F., Kasaya, M., Kasuya, T. & Date, M. Field-induced metallic state in YbB_{12} under high magnetic field. *J. Phys. Soc. Japan* **57**, 3946–3953 (1988).
9. Iga, F. et al. Anisotropic magnetoresistance and collapse of the energy gap in $Yb_{1-x}Lu_xB_{12}$. *J. Phys. Conf. Ser.* **200**, 012064 (2010).
10. Terashima, T. T. et al. Magnetic-field-induced Kondo metal realized in YbB_{12}. *Phys. Rev. Lett.* **120**, 257206 (2018).
11. Miyake, K. de Haas-van Alphen oscillations in superconducting states as a probe of gap anisotropy. *Physica B Condens. Matter* **186-188**, 115–117 (1993).
12. Knolle, J. & Cooper, N. R. Quantum oscillations without a Fermi surface and the anomalous de Haas-van Alphen effect. *Phys. Rev. Lett.* **115**, 146401 (2015).
13. Riseborough, P. S. & Fisk, Z. Critical examination of quantum oscillations in SmB_6. *Phys. Rev. B* **96**, 195122 (2017).
14. Peters, R., Yoshida, T. & Kawakami, N. Quantum oscillations in strongly correlated topological Kondo insulators. *Phys. Rev. B* **100**, 085124 (2019).
15. Zhang, L., Song, X. Y. & Wang, F. Quantum oscillation in narrow-gap topological insulators. *Phys. Rev. Lett.* **116**, 046404 (2016).
16. Lee, P. A. Quantum oscillations in the activated conductivity in excitonic insulators: possible application to monolayer WTe_2. *Phys. Rev. B* **103**, L041101 (2021).
17. Liu, J. & Balents, L. Correlation effects and quantum oscillations in topological nodal-loop semimetals. *Phys. Rev. B* **95**, 075426 (2017).
18. Bulaevskii, L. N., Batista, C. D., Mostovoy, M. V. & Khomskii, D. I. Electronic orbital currents and polarization in Mott insulators. *Phys. Rev. B* **78**, 024402 (2008).
19. Motrunich, O. I. Orbital magnetic field effects in spin liquid with spinon Fermi sea: possible application to κ-$(ET)_2Cu_2(CN)_3$. *Phys. Rev. B* **73**, 155115 (2006).
20. Baskaran, G. Majorana Fermi sea in insulating SmB_6: a proposal and a theory of quantum oscillations in Kondo insulators. Preprint at [https://arxiv.org/abs/1507.03477] (2015).
21. Erten, O., Chang, P. Y., Coleman, P. & Tsvelik, A. M. Skyrme insulators: insulators at the brink of superconductivity. *Phys. Rev. Lett.* **119**, 057603 (2017).
22. Varma, C. M. Majoranas in mixed-valence insulators. *Phys. Rev. B* **102**, 155145 (2020).
23. Chowdhury, D., Sodemann, I. & Senthil, T. Mixed-valence insulators with neutral Fermi surfaces. *Nat. Commun.* **9**, 1766 (2018).
24. Settai, R. et al. Quasi-two-dimensional Fermi surfaces and the de Haas-van Alphen oscillation in both the normal and superconducting mixed states of $CeCoIn_5$. *J. Phys. Condens. Matter* **13**, L627–L634 (2001).
25. Hedo, M. et al. Magnetoresistance and de Haas-van Alphen oscillation in normal and superconducting $CeRu_2$. *Philos. Mag. B* **77**, 975–1000 (1998).
26. Inada, Y. et al. Fermi surface and de Haas-van Alphen oscillation in both the normal and superconducting mixed states of UPd_2Al_3. *J. Phys. Soc. Japan* **68**, 3643–3654 (1999).
27. Ohkuni, H. et al. Fermi surface properties and de Haas-van Alphen oscillation in both the normal and superconducting mixed states of URu_2Si_2. *Philos. Mag. B* **79**, 1045–1077 (1999).
28. Clayton, N. J. et al. Superconducting fluctuations and the reduced dimensionality of the organic superconductor κ-$(BEDT\text{-}TTF)_2Cu(NCS)_2$ as observed through measurements of the de Haas-van Alphen effect. *Phys. Rev. B* **65**, 064515 (2002).
29. Werheit, H. et al. Raman scattering and isotopic phonon effects in dodecaborides. *J. Phys. Condens. Matter* **23**, 065403 (2011).
30. Iga, F., Shimizu, N. & Takabatake, T. Single crystal growth and physical properties of Kondo insulator YbB_{12}. *J. Magn. Magn. Mater.* **177-181**, 337–338 (1998).
31. Altarawneh, M. M., Mielke, C. H. & Brooks, J. S. Proximity detector circuits : an alternative to tunnel diode oscillators for contactless measurements in pulsed magnetic field environments. *Rev. Sci. Instrum.* **80**, 066104 (2009).
32. Blaha, P., Schwarz, K., Madsen, G., Kvasnicka, D. & Luitz, J. *WIEN2k: an augmented plane wave + local orbitals program for calculating crystal properties*. (Vienna University of Technology Institute of Materials Chemistry, Vienna, 2001).
33. Tran, F. & Blaha, P. Accurate band gaps of semiconductors and insulators with a semilocal exchange-correlation potential. *Phys. Rev. Lett.* **102**, 226401 (2009).
34. Anisimov, V. I., Zaanen, J. & Andersen, O. K. Band theory and Mott insulators: Hubbard *U* instead of Stoner *I*. *Phys. Rev. B* **44**, 943 (1991).
35. Shoenberg, D. *Magnetic oscillations in metals* (Cambridge University Press, Cambridge, UK, 1984).
36. Chang, T. R. et al. Two distinct topological phases in the mixed-valence compound YbB_6 and its differences from SmB_6. *Phys. Rev. B* **91**, 155151 (2015).

ACKNOWLEDGEMENTS

H.L., A.J.H., M.H., A.J.D., A.G.E., and S.E.S. acknowledge support from the Royal Society, the Leverhulme Trust through the award of a Philip Leverhulme Prize, the Winton Programme for the Physics of Sustainability, the Taiwanese Ministry of Education, EPSRC UK (studentship and grant numbers EP/M506485/1, EP/P024947/1, EP/1805236, EP/2124504), the Royal Society of Chemistry (researcher mobility grant M19-1108), and the European Research Council under the European Union's Seventh Framework Programme (Grant Agreement numbers 337425 and 772891). M.D.J. acknowledges support for this project by the Office of Naval Research (ONR) through the Naval Research Laboratory's Basic Research Programme. M.C.H. and G.B. acknowledge financial support from EPSRC, UK through Grant EP/T005963/1. We thank the team at the National Academy of Sciences of Ukraine, Kiev for assistance in the preparation of polycrystalline YbB_{12}. A portion of magnetic measurements were carried out using the Advanced Materials Characterisation Suite in the University of Cambridge, funded by EPSRC Strategic Equipment Grant EP/M000524/1.
We acknowledge support from the Deutsche Forschungsgemeinschaft (DFG) through the Würzburg-Dresden Cluster of Excellence on Complexity and Topology in Quantum Matter-ct.qmat (EXC 2147, Project No. 390858490) as well as the support of the HLD at HZDR, a member of the European Magnetic Field Laboratory (EMFL). A portion of this work was performed at the National High Magnetic Field Laboratory, which is supported by National Science Foundation Cooperative Agreement No. DMR-1157490, the State of Florida and the DOE.

AUTHOR CONTRIBUTIONS

H.L., A.J.H., M.H., A.J.D., A.G.E., T.E., E.P., T.H.V., V.W., G.G.L., and S.E.S. conducted the experiments and analyzed the results, N.S., M.C.H., and G.B. grew single crystal

samples, M.D.J. performed bandstructure calculations, T.F., J.W., and T.P.M. provided support for high field experiments, S.E.S. and H.L. wrote the manuscript with inputs from co-authors, S.E.S. designed and oversaw the project.

COMPETING INTERESTS

The authors declare no competing interests.

ADDITIONAL INFORMATION

Supplementary information The online version contains supplementary material available at https://doi.org/10.1038/s41535-021-00413-7.

Correspondence and requests for materials should be addressed to Suchitra E. Sebastian.

Reprints and permission information is available at http://www.nature.com/reprints

Publisher's note Springer Nature remains neutral with regard to jurisdictional claims in published maps and institutional affiliations.